Pattern analysis of computer keystroke time series in healthy control and early-stage Parkinson's disease subjects using fuzzy recurrence and scalable recurrence network features

Tuan Pham

Pham, T., (2018), Pattern analysis of computer keystroke time series in healthy control and early-stage Parkinson's disease subjects using fuzzy recurrence and scalable recurrence network features, *Journal of Neuroscience Methods*, 108(7), 1601-1622. https://doi.org/10.1016/j.jneumeth.2018.05.019

Pattern Analysis of Computer Keystroke Time Series in Healthy Control and Early-Stage Parkinson's Disease Subjects using Fuzzy Recurrence and Scalable Recurrence Network Features

Tuan D. Pham

Department of Biomedical Engineering

Linkoping University, Linkoping 58183, Sweden

Phone: +46-13-286778

E-mail: tuan.pham@liu.se

Abstract

Background: Identifying patients with early stages of Parkinson's disease (PD) in a home environment is an important area of neurological disorder research, because it is of therapeutic and economic benefits to optimal intervention and management of the disease. New Method: This paper presents a nonlinear dynamics approach, including recurrence plots, recurrence quantification analysis, fuzzy recurrence plots, and scalable recurrence networks for visualization, classification, and characterization of keystroke time series obtained from healthy control (HC) and early-stage PD subjects. Results: Several differentiative properties for characterizing early PD and HC subjects can be obtained from fuzzy recurrence plots (FRPs) and scalable recurrence networks. Comparison with Existing Methods: Cross-validation results obtained from FRP-based texture is highest among other methods. The method of fuzzy recurrence plots outperforms other existing methods for classification of HC and PD subjects. Conclusions: Features extracted from the nonlinear dynamics analysis of the keystroke time series are found to be very effective for machine learning and the prop-

erties of the scalable recurrence networks have the potential to be utilized as physiologic markers of the disease.

Keywords: Early Parkinson's disease, keystroke time series, fuzzy recurrence plots, scalable recurrence networks, texture analysis, pattern classification.

1 Introduction

In scientific terms, Parkinson's disease (PD) is a degenerative condition of the central nervous system that belongs to movement disorders. The precise cause of PD is still unknown, although some cases of PD are thought to be hereditary and can be the consequence of specific genetic mutations. According to the NIH National Institute of Neurological Disorders and Strokes (https://www.ninds.nih.gov), there is currently no cure for PD, and on-going research in PD is carried out along with the hope that medications or surgery such as deep brain stimulation can substantially improve the motor system of the brain.

While symptoms and progression of PD are unique to each individual, patterns of progression in PD can be generally classified into five stages to describe the severity of the disease based on the Hoehn and Yahr Scale [1]. Stage 1 shows tremor and other movement symptoms on one side of the body without functional impairment. Stage 2 involves first signs of tremor and other movement symptoms on both sides of the body without impairment of balance. Stage 3 shows loss of balance and slowness of movement that fail to protect against falling. Stage 4 shows severe disability of standing and walking. Stage 5 causes stiffness in the legs and restricts the patient to bed or wheelchair. Stages between 1 and 2 are of early onset, between 2 and 3 of intermediate phase, and between 4 and 5 of advanced PD.

It is difficult to tell if someone has PD, particularly in its early stages. Based on the current information from the Parkinson's Foundation (http://parkinson.org/ understanding-parkinsons/10-early-warning-signs), signs that can reveal the symptoms of PD are the combinations of tremor, small handwriting, loss of smell, trouble sleeping, trouble moving or walking, constipation, soft or low voice, masked face (expressing a depressed or mad look), dizziness or fainting, and stooping when standing.

In addition to the use of electroencephalography and electrooculography for studying PD [2], and analysis of cortical recordings obtained during deep brain stimulation for treating neurological and psychiatric disorders [3], there are several other informatics-based studies of PD using physiological signals, mostly being concerned with pattern analysis and classification of gait dynamics of healthy control (HC) subjects and PD patients. Studies about gait characteristics in PD are often carried out using sensor-based data [4]. Other typical research reports include the application of the non-parametric Parzen window method and machine learning for determining the stride properties of the gait time series to differentiate between HC and PD groups [5], the use of fractal methods that were implemented to analyze long time series of strides to classify healthy control (HC) and PD groups [6], and the development of gait asymmetry measures with the wavelet transform for decomposing vertical ground reaction force time series of the left and right feet to evaluate the difference in gait asymmetry between the control and PD subjects [7].

More recent reports include the development of an anomaly-based algorithm for predicting gait freeze from skin-conductance features extracted from wearable sensor data recorded from patients with advanced PD [8], applications of several machine-learning methods trained with spatial-temporal gait data during self-selected walking to classify PD patients and aged-

matched control subjects [9], complexity analysis of gait dynamics in aging and PD groups [10], and the utilization of a deterministic learning approach for differentiating HC from PD subjects [11]. Some most recent works include use of the empirical mode decomposition and classification techniques for analyzing gait dynamics in neuro-degenerative diseases and stratifying individuals into HC, PD, Huntington's disease (HD), and amyotrophic lateral sclerosis (ALS) groups [12], tensor decomposition of gait force data in PD [13], and the application of fuzzy recurrence plots for extracting texture features from the time series of stride intervals to classify PD, HD, and ALS from HC subjects [14].

As a different study from gait dynamics analysis, the classification of motor signs recorded from patients with early-stage PD from HC subjects using time series of computer-key hold times was carried out using ensemble regression [15]. The study in this paper attempts to apply advanced nonlinear dynamics methods to analyze the same database of the computer-key hold times to discover new findings in differentiating the routine interaction of early-stage PD patients from HC subjects with computer keyboards. While the work reported in [14] applied the concept of texture analysis of fuzzy recurrence plots of stride-interval time series, the findings presented in this paper present the potential application of the fuzzy recurrence plot method and scalable recurrence networks, which are newly developed algorithms for nonlinear data analysis, to a different data type for studying PD in its early stage. The novel aspects of this paper are: (1) the proposed methods outperformed those that have been most recently reported in literature for the classification of early PD and HC subjects using the same dataset; (2) for the first time, two-dimensional analysis of computer keystroke time series is carried out using fuzzy recurrence plots and scalable recurrence networks; and (3) in particular, the concept of scalable recurrence networks has recently been proposed in

[16] but never been applied to studying real-life time series elsewhere.

The rest of this paper is organized as follows. Sections 2-4 briefly describe the methods addressed in this study that are recurrence plots, recurrence quantification analysis, fuzzy recurrence plots, and scalable recurrence networks, respectively. Section 5 describes the PhysioNet database used in this study. Section 6 presents the results. Section 7 is the discussion of the results and findings. Finally, Section 8 is the conclusion of the paper, reflecting upon the findings and issues suggested for further research.

2 Recurrence plots and recurrence quantification analysis

A recurrence plot (RP) [17] is a visualization method for studying patterns of chaos in time series. An RP shows the times at which a phase-space trajectory approximately revisits the same area in the phase space. Let $X = \{x\}$ be a set of phase-space states, in which x_i is the i-th state of a dynamical system in m-dimensional space and time delay δ. An RP is constructed as an $N \times N$ matrix in which an element (i, j), $i = 1, \ldots, N$, $j = 1, \ldots, N$, is represented with a black dot if x_i and x_j are considered to be closed to each other. For a symmetrical RP, a threshold, denoted as ϵ, is used to define the similarity of a state pair (x_i, x_j) as follows [18]

$$R(i, j) = H[d(x_i, x_j)], \tag{1}$$

where $R(i,j)$ is an element (i,j) of the recurrence matrix R, $d(x_i, x_j)$ is a distance function of x_i and x_j, and $H(\cdot)$ is the Heaviside function expressed as

$$H[d(x_i, x_j)] = \begin{cases} 1 & : d(x_i, x_j) \leq \epsilon \\ 0 & : d(x_i, x_j) > \epsilon \end{cases} \tag{2}$$

Based on an RP defined in Eq. (1), several recurrence quantification analysis (RQA) measures of the RP structure complexity can be determined. These RQA measures include [18, 19, 20, 21]: recurrence rate, determinism, mean diagonal line length, maximal diagonal line length, entropy of the diagonal line lengths, laminarity, trapping time, maximal vertical line length, recurrence time of the first type, recurrence time of the second type, and recurrence time entropy.

3 Fuzzy recurrence plots

A fuzzy recurrence plot (FRP) [22] is an extension of an RP, where the output of the former results in a grayscale image and the latter is a binary one. An FRP constructs the recurrence image that takes values in $[0, 1]$ without requiring the similarity threshold parameter ϵ needed for the RP analysis. The formulation of an FRP is described as follows [22].

Let $V = \{v\}$ be the set of fuzzy clusters of the states. A binary relation R from X to V is a fuzzy subset of $X \times V$ characterized by a fuzzy membership function $\mu \in [0, 1]$. This fuzzy membership grade expresses the degree of relation of each pair (x, v) in R that has the following properties [23]:

- Reflexivity: $\mu(x, x) = 1$, $\forall x \in X$,

- Symmetry: $\mu(x, v) = \mu(v, x)$, $\forall x \in X, \forall v \in V$, and
- Transitivity: $\mu(x, z) = \vee_v[\mu(x, v) \wedge \mu(v, z)]$, $\forall x \in X, \forall z \in Z$, which is called the max-min composition, where the symbols $\vee$ and $\wedge$ stand for max and min, respectively.

By specifying a number of clusters c for the data, the fuzzy c-means algorithm [24] is applied to identify the fuzzy clusters of the phase-space states and determine the similarity between the states and the fuzzy cluster centers. Based on this direct similarity measure, the inference of the similarity between the pairs of the states can be carried out using the max-min composition of a fuzzy relation.

For feature extraction, the gray-level co-occurrence matrix (GLCM) [25] can be applied to quantify the textural properties of an FRP. The GLCM of a gray-scale image of size $M_1 \times M_2$ is a function of two gray-scale variables p and q with a geometric offset $\Delta = (\Delta h, \Delta v)$ in row-wise (h) and column-wise (v) directions of a gray-scale image, denoted as $G_\Delta(p, q)$ and defined as

$$G_\Delta(p, q) = \sum_{h=1}^{M_1} \sum_{v=1}^{M_2} [I(h, v) = p] \wedge [I(h + \Delta h, v + \Delta v) = q], \tag{3}$$

where $I(h, v)$ and $I(h + \Delta h, v + \Delta v)$ are pixels at locations (h, v) and $(h + \Delta h, v + \Delta v)$, $p, q \in [0, 255]$, and $\wedge$ stands for the logical AND operator.

The derived probabilities of the GLCM defined in Eq. (3) allow the extraction of a variety of features, including [25, 26, 27]: autocorrelation, cluster prominence, cluster shade, contrast, correlation, difference entropy, difference variance, dissimilarity, energy, entropy, homogeneity, information measure of correlation 1, information measure of correlation 2, inverse difference, maximum probability, sum average, sum entropy, sum of squares variance,

and sum variance.

4 Scalable recurrence networks

The construction of a scalable recurrence network [16] from a FRP is presented as follows. An α-cut FRP is a binary recurrence matrix, denoted as FRM_α, which can be defined as

$$FRM_\alpha = \begin{cases} 0 & : \mu(x,z) \geq \alpha \\ 1 & : \text{otherwise} \end{cases} \tag{4}$$

where $\alpha \in [0,1]$, and 0 and 1 indicate black and white pixels, respectively.

The adjacency matrix of an undirected and unweighted α-cut recurrence network, denoted as R_α, can be expressed as

$$R_\alpha = FRM_\alpha - I. \tag{5}$$

where I is an identity matrix.

It is desirable to make a recurrence network scalable to enable its visualization and reduce its computational complexity. The scalability of the adjacency matrix of an undirected α-cut recurrence network can be obtained by replacing the phase-space states with a number of phase-space prototypes, denoted as c, which are the number of fuzzy cluster centers. By using the fuzzy relation to infer the fuzzy membership grades of similarity between the cluster pairs $(\phi, \theta) \in V$, the following properties can be obtained:

- $\mu(\phi,\phi) = 1,\ \forall \phi \in V.$
- $\mu(\phi,x) = \mu(x,\phi),\ \forall \phi \in V, \forall x \in X.$

- $\mu(\phi, \theta) = \vee_x[\mu(\phi, x) \wedge \mu(x, \theta)]$, $\forall \phi, \theta \in V$.

A β-cut prototype recurrence matrix of size $c \times c$, denoted as M_β, can be obtained by

$$M_\beta = \begin{cases} 1 & : \mu(\phi, \theta) \geq \beta \\ 0 & : \text{otherwise} \end{cases} \tag{6}$$

where $\beta \in [0, 1]$.

Finally, the adjacency matrix of a scalable recurrence network, denoted as B_β, is defined as

$$B_\beta = M_\beta - I. \tag{7}$$

While the selection of the number of clusters c can be arbitrarily selected for constructing an FRP as it is not critical as studied in [22]. For the construction of a scalable recurrence network, the number of clusters c represent the number of nodes of the network and can be estimated using a cluster validity measure such as the partition entropy, denoted by H, which is defined as [24]

$$H = \frac{1}{M} \sum_{j=1}^{c} \sum_{i=1}^{M} \mu_{ij} \log(\mu_{ij}). \tag{8}$$

Given a maximum number of clusters, the cluster validity computes the partition entropy H for each cluster size, $c \geq 2$, then selects the number of clusters that has the minimum value of H as an optimal c for the FCM algorithm.

Two popular measures of a network are the average clustering coefficient and the characteristic path length [28]. The average clustering coefficient, denoted as $< CC >$, for an adjacency matrix A of size $N \times N$ of an undirected and unweighted graph is defined as

$$< CC >= \frac{1}{N} \sum_{i=1}^{N} C_i, \tag{9}$$

where

$$C_i = \frac{\sum_{j,k=1}^{N} A_{ij} A_{jk} A_{ki}}{l_i(l_i - 1)}, \tag{10}$$

where

$$l_i = \sum_{j=1}^{N} A_{ij}. \tag{11}$$

The characteristic path length, denoted as CPL, which is the average shortest path of an undirected and unweighted graph is defined as

$$CPL = \frac{1}{N(N-1)} \sum_{i \neq j, i, j=1}^{N} d_{ij} \tag{12}$$

where d_{ij} is the length of the shortest path between nodes i and j.

5 Dataset

The computer-key hold time series, which are series of the hold times occurring between pressing and releasing a computer key while the user is typing in a standard word processor, used in this study are included in the neuroQWERTY MIT-CSXPD dataset. This database is publicly available on the PhysioNet (https://www.physionet.org/physiobank/database/nqmitcsxpd/). This database contains keystroke time series obtained from healthy control (HC) subjects and patients with early-stage Parkinson's disease (PD) recruited from two movement disorder units in Spain following the institutional protocols approved by institutions in the USA

and Spain. Each data file includes the timing information collected during the sessions of typing activity using a standard word processor on a Lenovo G50-70 i3-4005U. The subjects were instructed to type as they normally would do at home and they were left free to correct typing mistakes. The key acquisition software presented a temporal resolution of 3/0.28 (mean/standard deviation) milliseconds. The combined data include 56 computer-key hold time series recorded from 43 HC subjects, and 60 computer-key hold time series recorded from 42 early-stage PD patients. In addition, clinical evaluations were performed on each subject, including Unified Parkinson's Disease Rating Scale (UPDRS) [29] and finger tapping tests [15].

6 Results

Due to outliers existing in the raw time series of the HC and PD individuals, where several data points are in the magnitude of 10^9, those huge values were removed from the time series before carrying out the task of feature extraction. To extract RQA features, the RPs of the HC and PD individuals were first computed with embedding dimension $m = 1$, time delay $\delta = 1$, and similarity threshold $\epsilon = 0.05 \times \mu(\mathbf{x})$, where $\mathbf{x}$ is the time series of each individual, and $\mu(\mathbf{x})$ is the mean of $\mathbf{x}$. Eleven RQA features extracted from the RPs are recurrence rate (RR), determinism (DET), mean diagonal line length ($< L >$), maximal diagonal line length ($L_{\max}$), entropy of the diagonal line lengths (ENT), laminarity (LAM), trapping time (TT), maximal vertical line length ($V_{\max}$), recurrence time of the first type (T_1), recurrence time of the second type (T_2), and recurrence time entropy (RTE). Both minimal diagonal line length $L_{\min}$ and minimal vertical line length $V_{\min}$ were set to 2.

To extract FRP-based GLCM features, the FRPs of the HC and PD individuals were first computed with embedding dimension $m = 1$, time delay $\delta = 1$, and the number of clusters $c = 5$ that was chosen to reflect a reasonable representation of texture of FRPs. Nineteen GLCM-based features were extracted from the FRPs, which are: autocorrelation, cluster prominence, cluster shade, contrast, correlation, difference entropy, difference variance, dissimilarity, energy, entropy, homogeneity, information measure of correlation 1, information measure of correlation 2, inverse difference, maximum probability, sum average, sum entropy, sum of squares variance, and sum variance. The orientation for computing the GLCM is one pixel to the right, which indicates $\Delta = [0, 1]$.

To compute various values of the $< CC >$ (the average clustering coefficient) and CPL (the characteristic path length), the scalable recurrence networks of the HC and PD individuals were constructed with the number of clusters $c = 20$ (estimated from the validity measure defined in Eq. (8)), $\alpha = 0.5$, and $\beta = 0.01$, 0.05, and 0.1.

The means and standard deviations of 11 RQA features for the HC and PD groups are shown in Table 1. The means and standard deviations of 19 FRP-based GLCM features for the HC and PD groups are shown in Table 2. The Pearson's correlation coefficient for the 11 RQA features of the HC and PD is 1 with the corresponding p-value of zero to the twenty digits, whereas the Pearson's correlation coefficient for the 19 GLCM features of the HC and PD is 0.9960 with the corresponding p-value of zero to the eighteen digits. Such values indicate a very strong correlation between the HC and PD features, and suggest better discriminating power of the GLCM features extracted from fuzzy recurrence plots.

The two-fold cross-validations of the classification of the HC subjects and PD patients using the least-squares support vector machines (LS-SVM) [30] was repeated 10 times. The LS-

SVM was adopted in this study because of its best performance among several other classifiers recently reported in [14]. The mean values of the receiver operating characteristics (ROC) obtained from the RQA and FRP-GLCM features, as well as the areas under the ROC curves (AUC) obtained from the numerical neuroQWERTY index (nQi) model [15], where nQi1 is the model using all non-overlapping windows of the time series, whereas nQi2 using each of the non-overlapping time windows, alternating finger tapping (AFT) [31], and single key tapping (SKT) [32], are shown in Table 3. The 10 results of the two-fold cross-validations obtained from RQA were among the three values of AUC, specificity, sensitivity, and accuracy as shown in Table 4. Furthermore, Table 5 shows the ten-fold and leave-one-out (LOO) cross-validations results obtained from the RQA and FRP-GLCM. Figure 1 shows the plots of the receiver operating characteristic (ROC) curves for the ten-fold and LOO cross-validations obtained from the RQA and FRP-GLCM (ROC curve with AUC = 1 for the LOO cross-validation obtained from the FRP-GLCM is not plotted).

Figures 2 and 3 show the computer-key hold time series, RP, FRP, and three scalable recurrence networks of an HC subject and a patient diagnosed with early-stage PD. Table 6 shows the mean values of $< CC >$ and CPL obtained from scalable recurrence networks using three different values for β for the HC and PD groups, where the p-values for the $< AC >$ and CPL of both HC and PD groups are $< 10^{-59}$.

7 Discussion

Based on the two-fold cross-validations for the classification of 56 key-hold time series of the HC group and 60 key-hold time series of the early-stage PD group, results obtained from

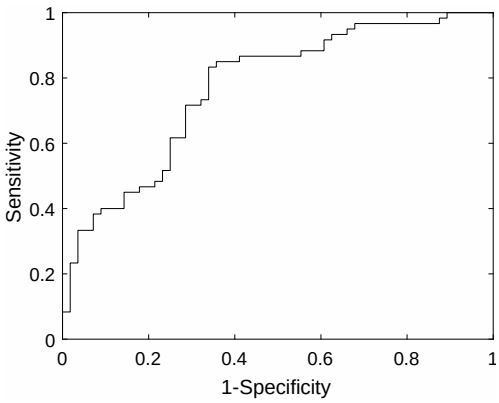

(a) RQA (10-fold)

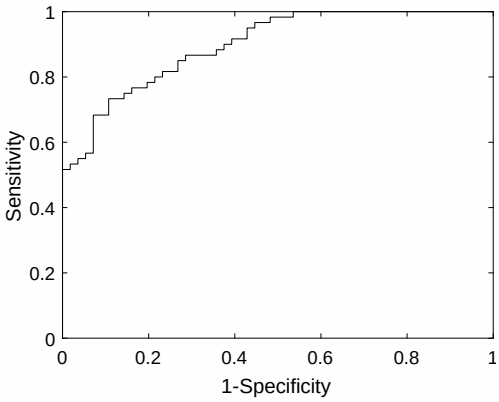

(b) FRP-GLCM (10-fold)

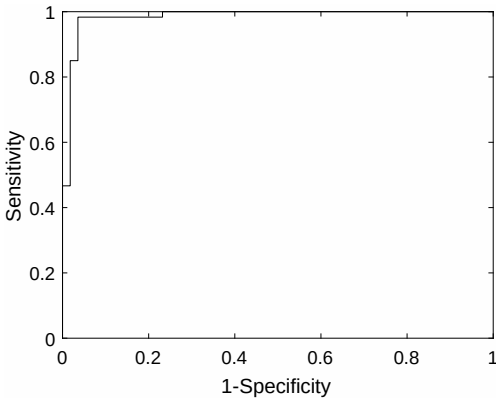

(c) RQA (LOO)

Figure 1: ROC curves for cross-validations obtained from RQA and FRP-GLCM: AUCs = 0.77 (a), 0.89 (b), and 0.98 (c).

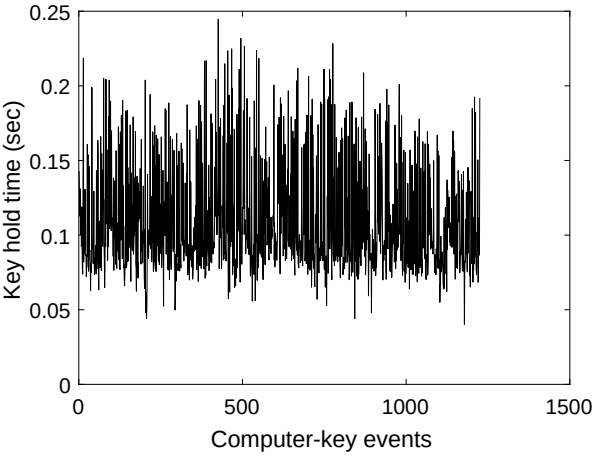

(a) Time series

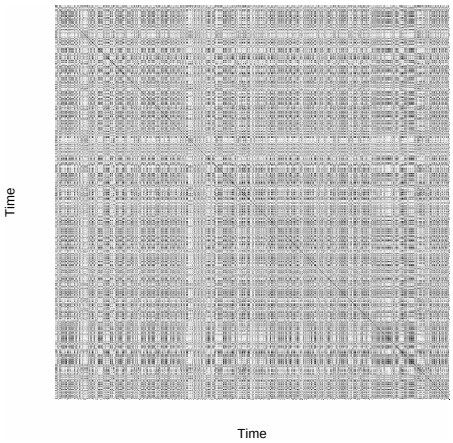

(b) FRP

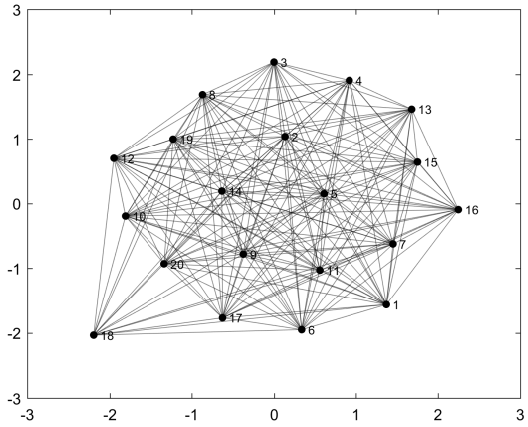

(c) β=0.01

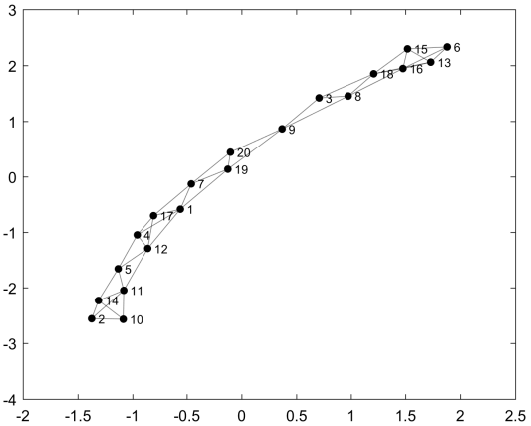

(d) β=0.05

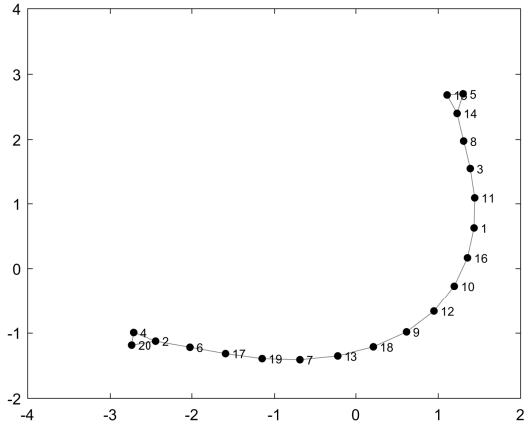

(e) β=0.1

Figure 2: (a) Time series of computer-key hold time recorded from an HC subject, its (b) fuzzy recurrence plot (FRP), and (c)-(e) scalable recurrence networks.

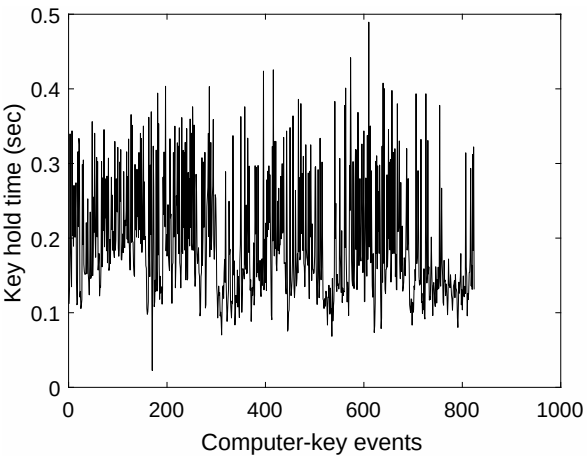

(a) Time series

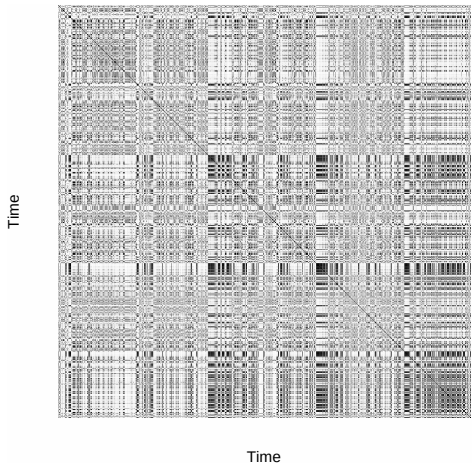

(b) FRP

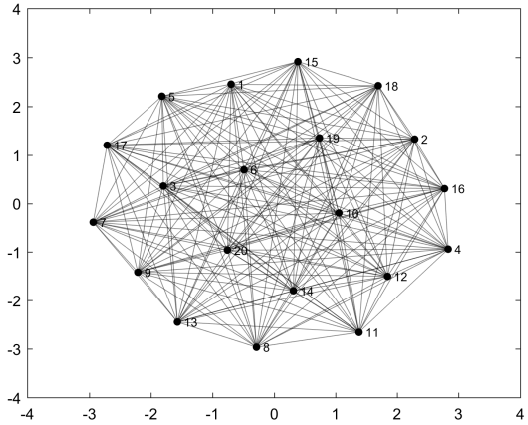

(c) β=0.01

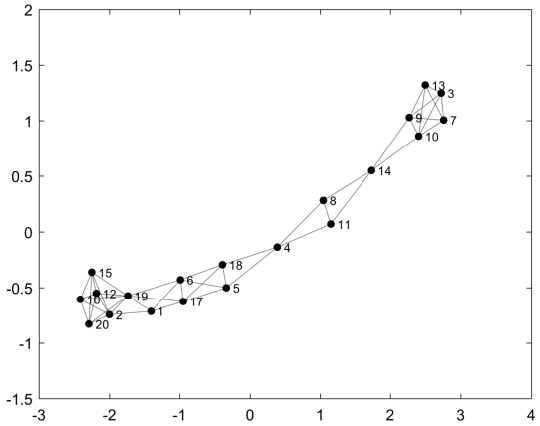

(d) β=0.05

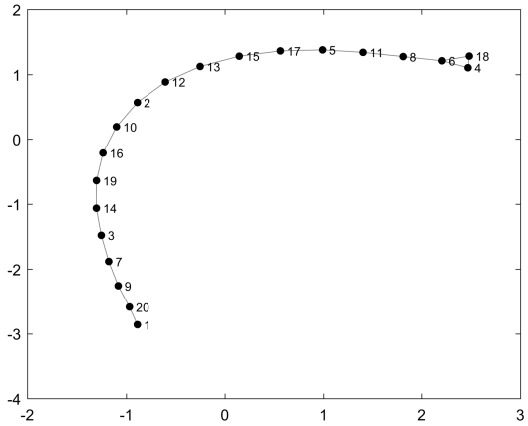

(e) β=0.1

Figure 3: (a) Time series of computer-key hold time recorded from an early PD patient, its (b) fuzzy recurrence plot (FRP), and (c)-(e) scalable recurrence networks.

Table 1: Means and standard deviations of 11 RQA features for healthy control (HC) and Parkinson's disease (PD) groups, with p-values $< 0.8 \times 10^{-6}$ for HC and p-values < 0.0001 for PD features.

Feature	HC	PD
RR	0.0256 $\pm$0.0320	0.0252 $\pm$0.0468
DET	0.0523 $\pm$0.0614	0.0502 $\pm$0.0826
$< L >$	2.0307 $\pm$0.0415	2.0326 $\pm$0.0671
$L_{\max}$	3.2679 $\pm$1.3002	3.1833 $\pm$1.5784
ENT	0.0166 $\pm$0.0080	0.0171 $\pm$0.0077
LAM	0.0722 $\pm$0.0797	0.0688 $\pm$0.1002
TT	2.0458 $\pm$0.0721	2.0455 $\pm$0.1053
$V_{\max}$	3.0357 $\pm$1.4008	2.9500 $\pm$1.5341
T_1	95.6265 $\pm$82.0043	79.3590 $\pm$47.8122
T_2	97.3062 $\pm$82.2440	80.9654 $\pm$47.8072
RTE	0.1265 $\pm$0.0222	0.1321 $\pm$0.0208

using either the RQA or FRP-based GLCM features for training the LS-SVM outperform those provided by the nQi model [15], alternating finger tapping (AFT) [31], and single key tapping (SKT) [32], where the AUCs = 0.81, 0.79, 0.75, 0.61, 0.96, and 1 for nQi1, nQi2, AFT, SKT, RQA, and FRP-GLCM, respectively (Table 3). The FRP-GLCM not only outperformed the RQA in the two-fold cross-validation (Table 3), but also in the ten-fold

Table 2: Means and standard deviations of 19 FRP-based GLCM features, where F1 = autocorrelation, F2 = cluster prominence, F3 = cluster shade, F4 = contrast, F5 = correlation, F6 = difference entropy, F7 = difference variance, F8 = dissimilarity, F9 = energy, F10= entropy, F11 = homogeneity, F12 = information measure of correlation 1, F13 = information measure of correlation 2, F14 = inverse difference, F15 = maximum probability, F16 = sum average, F17 = sum entropy, F18 = sum of squares variance, and F19 = sum variance, with p-values < 0.00001 for HC and p-values $< 0.8 \times 10^{-7}$ for PD features.

Cohort	F1	F2	F3	F4	F5
HC	29.6339 ±10.5189	573.1053 ±172.1820	-12.5450 ±30.4113	11.0616 ±2.6468	0.1372 ±0.1315
PD	30.5137 ±8.8956	631.0476 ±211.4640	-20.8186 ±24.7021	11.5710 ±2.7627	0.1507 ±0.1154
Cohort	F6	F7	F8	F9	F10
HC	1.7429 ±0.3568	5.9607 ±1.0870	2.2015 ±0.5086	0.1238 ±0.1723	3.1969 ±0.7053
PD	1.7467 ±0.2990	6.2731 ±1.2286	2.2573 ±0.4539	0.1133 ±0.1439	3.2030 ±0.5959
Cohort	F11	F12	F13	F14	F15
HC	0.5165 ±0.1120	-0.0850 ±0.0661	0.4537 ±0.1118	0.5746 ±0.0984	0.2707 ±0.1778
PD	0.5134 ±0.0921	-0.0796 ±0.0476	0.4546 ±0.0979	0.5717 ±0.0810	0.2652 ±0.1446
Cohort	F16	F17	F18	F19	
HC	10.4377 ±2.5315	2.2374 ±0.4450	6.3543 ±1.3605	14.3587 ±3.4359	
PD	10.6593 ±2.1010	2.2621 ±0.3803	6.8090 ±1.5609	15.6643 ±4.2168	

and LOO cross-validations (Table 5). Regarding the RQA features (Table 1), T_1 (recurrence time of the first type), having 96 for the HC and 79 for the PD, and T_2 (recurrence time of the second type), having 97 for the HC and 81 for the PD, are the most differentiating features. As for the FRP-based GLCM features (Table 2), F2 (cluster prominence), taking 573 for

Table 3: Mean two-fold cross-validation results for classification of healthy control and early-stage Parkinson's disease subjects obtained from different methods in terms of sensitivity (SEN), specificity (SPE), area under ROC curve (AUC), and accuracy (ACC), where 'N/A' indicates not available.

Method	AUC	SEN (%)	SPE (%)	ACC (%)
nQi1	0.81	71.00	84.00	78.00
nQi2	0.79	N/A	N/A	N/A
AFT	0.75	N/A	N/A	N/A
SKT	0.61	N/A	N/A	N/A
RQA	0.96	93.50	90.18	91.90
FRP-GLCM	1	100	100	100

Table 4: Variation of two-fold cross-validation results for classification of healthy control and early-stage Parkinson's disease subjects obtained from RQA in terms of sensitivity (SEN), specificity (SPE), area under ROC curve (AUC), and accuracy (ACC).

AUC	SEN (%)	SPE (%)	ACC (%)
0.93	90.00	82.14	86.21
0.97	91.67	91.07	91.38
1	100	100	100

Table 5: Cross-validation results for classification of healthy control and early-stage Parkinson's disease subjects obtained from RQA and FRP-GLCM in terms of sensitivity (SEN), specificity (SPE), area under ROC curve (AUC), and accuracy (ACC).

Method	AUC	SEN (%)	SPE (%)	ACC (%)
Ten-fold cross-validation				
RQA	0.77	71.67	71.43	70.00
FRP-GLCM	0.89	85.00	73.21	79.31
LOO cross-validation				
RQA	0.98	98.33	96.43	97.41
FRP-GLCM	1	100	100	100

the HC and 631 for the PD, and F3 (cluster shade), taking respective negative values of 13 and 21 for the HC and PD, are the most discerning features. The p-values of the RQA and FRP-GLCM features for both HC and PD groups as shown in Tables 1 and 2, respectively, are statistically highly significant. The RQA features are more statistically significant than the FRP-GLCM features for the HC group, whereas the FRP-GLCM features are more statistically significant than the RQA features for the PD group. The FRP-based GLCM features are most effective for classifying the computer keystroke time series recorded from the HC and PD groups as illustrated in the cross-validation results obtained from different methods.

In regard to visualization, the FRPs show much better visual representations of the time se-

Table 6: Mean values of average clustering coefficient ($< CC >$) and characteristic path length (CPL) obtained from scalable recurrence networks using different values for β for healthy control (HC) and Parkinson's disease (PD) groups.

HC		
β	$< CC >$	CPL
0.01	0.9917 ±0.0159	1.0230 ±0.0528
0.05	0.7345 ±0.0335	3.0935 ±1.8348
0.1	0.1806 ±0.0454	5.9369 ±3.8677
PD		
β	$< CC >$	CPL
0.01	0.9907 ±0.0067	1.0283 ±0.0509
0.05	0.7094 ±0.0266	3.3611 ±2.0335
0.1	0.1610 ±0.0496	6.1544 ±4.0275

ries than the RPs as illustrated in [22], where the similarity threshold ϵ was chosen according to a documented suggestion [18]. In fact, the selection of the number of clusters for an FRP has been found not to be as sensitive as for the selection of the parameter ϵ [22], allowing the ease of use of the FRP method. For the natural selection of the embedding dimension of 1 and time delay of 1 for one-dimensional signals, the use of the recurrence networks based on recurrence plots for time series of more than 1500 sample points is not desirable for the purpose of visualization. FRPs and scalable recurrence networks not only are effective

for the LS-SVM classification, but also useful for visualizing the characteristics of the time series. As a case as shown in Figures 2 and 3, while it can be difficult to differentiate the two time series (2 (a) and 3 (a)), difference in the recurrence patterns of the two groups can be more easily recognized by their FRPs (2 (c) and 3 (c)), where the texture of FRP of the HC subject is finer than that of the PD patient. Similarly, topologies of the three scalable recurrence networks of the time series of the HC subject (Figure 2 (d)-(f)) are also different from those of the PD patient (Figure 3 (d)-(f)).

The values for the $< CC >$ of the HC are consistently larger than those of the PD (Table 6), which indicate the vertices of the scalable recurrence networks of the HC are more connected than those of the PD. The values for the CPL of the HC are consistently smaller than those of the PD (Table 6), suggesting the vertices of the PD networks are connected with shorter paths than those of the HC networks. The larger value of β, the more separable values of $< CC >$ and CPL obtained for HC and PD groups. In this study, the increase of values for β was stopped at 0.1, because a higher value would result in the generation of mostly disconnected vertices of the networks. The p-values for the $< CC >$ and CPL of both HC and PD groups are almost zero, indicating a strong evidence of their statistical significance.

8 Conclusion

The extraction of nonlinear dynamics features using recurrence plots, fuzzy recurrence plots, and scalable recurrence networks for classifying and characterizing HC individuals from those with early-stage PD have been presented and discussed. The use fuzzy recurrence plots with an advanced machine learning method enable the power of the classification of this type

of signals. Particularly, fuzzy recurrence plots are rich in texture and therefore allow the exploration of many texture models for pattern classification, which is worth further investigation in future research applied to the analysis of complex and nonlinear keystroke time series. The number of clusters for constructing a fuzzy recurrence plot as well as values for parameter β for constructing scalable recurrence networks from fuzzy recurrence plots were heuristically chosen in this study. The development of some analytical or numerical methods for optimal selections of these two parameters would certainly advance the applications of the proposed approach.

For the construction of either a recurrence plot or a fuzzy recurrence plot, the selection of appropriate values for the time delay and embedding dimension, which are called the embedding parameters, is naturally sought. It is reported [33] that the most commonly adopted methods for estimating the time delay and embedding dimension are the average mutual information [34] and the false nearest neighbors [35], respectively. However, these two methods are heuristic and several other methods have been developed to provide alternative estimates for these embedding parameters [33]. It was shown that for low-dimensional systems, the same results for constructing recurrence plots can be obtained without the need for embedding [36]. Thus, the embedding parameters of one were used for the one-dimensional signals in this study. The partition entropy function expressed in Eq. (8) as used for constructing scalable recurrence networks can be applied for selecting an appropriate number of clusters for a fuzzy recurrence plot. The number of clusters selected in this study was based on a good appearance of texture of the fuzzy recurrence plots for the purpose of texture extraction. However, being similar to the study of the selection of the embedding parameters, the exploration of relationship between the classification performance and the selections of the

embedding parameters and number of clusters for constructing fuzzy recurrence plots from time series deserves study in its own right in future research.

Due to data availability, the proposed methods for analysis and classification of keystroke time series are limited to the study of healthy control and early-stage PD subjects. Extended applications of the proposed methods to studying PD subjects of different disease stages are certainly promising, because the pattern classification of signals measured from healthy control and early-stage PD subjects is supposed to be the most difficult task in comparison with PD subjects of more severe symptoms. In other words, patterns of motor signs in latter stages of PD would be easier for a classifier to recognize than those in an early onset of the disease. Likewise, extension of applications of the fuzzy recurrence plots and their scalable networks for differentiating physiological time series obtained from patients with PD, dementia, depression, and mixture of the diseases is promising to deliver effective results.

While the method of recurrence plots has been relatively a commonly applied method for studying time series, the potential of the newly developed method of fuzzy recurrence plots is still not widely explored for analysis of time series in physiology. Network-based analysis has been gaining increasing attention in medicine and biology [37, 38, 39, 40, 41]. For the first time, the method of scalable recurrence networks was adopted to investigate network properties of time series of motor signs measured from computer key hold times of early PD. It has been suggested that new biomarker discovery together with imaging techniques, clinical examinations and neuropathological assessments will lead to novel therapeutics for PD [42]. Comprehensive study of network-based measures addressed in this study will have an important implication as physiologic markers for early prognosis and therapeutic evaluation of the disease.

References

[1] M. Hoehn, M. Yahr, Parkinsonism: onset, progression and mortality, *Neurology*, vol. 17, pp. 427-442, 1967.

[2] J.A. Christensen, M. Zoetmulder, H. Koch, R. Frandsen, L. Arvastson, S.R. Christensen, P. Jennum, and H.B. Sorensen, Data-driven modeling of sleep EEG and EOG reveals characteristics indicative of pre-Parkinson's and Parkinson's disease, *J Neurosci Methods*, vol. 235, pp. 262-276, 2014.

[3] A. Oswal, A. Jha, S. Neal, A. Reid, D. Bradbury, P. Aston, P. Limousin, T. Foltynie, L. Zrinzo, P. Brown, and V. Litvak, Analysis of simultaneous MEG and intracranial LFP recordings during Deep Brain Stimulation: a protocol and experimental validation, *J Neurosci Methods*, vol. 261, pp. 29-46, 2016.

[4] J.C.M. Schlachetzki, J. Barth, F. Marxreiter, J. Gossler, Z. Kohl, S. Reinfelder, et al., Wearable sensors objectively measure gait parameters in Parkinson's disease, *PLoS ONE*, vol. 12, e0183989, 2017.

[5] Y. Wu, S. Krishnan, Statistical analysis of gait rhythm in patients with Parkinson's disease, *IEEE Trans Neural Systems and Rehabilitation Engineering*, vol. 18, pp. 150-158, 2010.

[6] M. Kirchner, P. Schubert, M. Liebherr, and C.T. Haas, Detrended fluctuation analysis and adaptive fractal analysis of stride time data in Parkinson's disease: Stitching together short gait trials, *PLoS ONE*, vol. 9, e85787, 2014.

[7] B.L. Su, R. Song, L.Y. Guo, and C.W. Yen, Characterizing gait asymmetry via frequency sub-band components of the ground reaction force, *Biomedical Signal Processing and Control*, vol. 18, 2015, pp. 56-60, 2015.

[8] S. Mazilu, A. Calatroni, E. Gazit, A. Mirelman, J.M. Hausdorff, and G. Troster, Prediction of freezing of gait in Parkinson's from physiological wearables: an exploratory study, *IEEE J Biomed Health Inform.*, vol. 19, pp. 1843-1854, 2015.

[9] F. Wahid, R.K. Begg, C.J. Hass, S. Halgamuge, and D.C. Ackland, Classification of Parkinson's disease gait using spatial-temporal gait features, *IEEE J Biomed Health Inform.*, vol. 19, pp. 1794-1802, 2015.

[10] C. Kamath, Analysis of altered complexity of gait dynamics with aging and Parkinson's disease using ternary Lempel-Ziv complexity, *Cogent Engineering*, vol. 3, 1177924, 2016.

[11] W. Zeng and C. Wang, Parkinson's disease classification using gait analysis via deterministic learning, *Neuroscience Letters*, vol. 633, pp. 268-278, 2016.

[12] P. Ren, S. Tang, F. Fang, L. Luo, L. Xu, M.L. Bringas-Vega, D. Yao, K.M. Kendrick, and P.A. Valdes-Sosa, Gait rhythm fluctuation analysis for neurodegenerative diseases by empirical mode decomposition, *IEEE Trans Biomedical Engineering*, vol. 64, pp. 52-60, 2017.

[13] T.D. Pham, H. Yan, Tensor decomposition of gait dynamics in Parkinson's disease, *IEEE Trans Biomedical Engineering*, published online 04 December 2017, DOI: 10.1109/TBME.2017.2779884.

[14] T.D. Pham, Texture classification and visualization of time series of gait dynamics in patients with neuro-degenerative diseases, *IEEE Trans Neural Syst Rehabil Eng*, vol. 26, pp. 188-196, 2018.

[15] L. Giancardo, A. Sanchez-Ferro, T. Arroyo-Gallego, I. Butterworth, C.S. Mendoza, P. Montero, M. Matarazzo, J.A. Obeso, M.L. Gray, and R. San Jose Estepar, Computer keyboard interaction as an indicator of early Parkinson's disease, *Scientific Reports*, vol. 6, 34468, 2016.

[16] T.D. Pham, From fuzzy recurrence plots to scalable recurrence networks of time series, *EPL (Europhysics Letters)*, vol. 118, 20003, 2017.

[17] J.P. Eckmann, S.O. Kamphorst, and D. Ruelle, Recurrence plots of dynamical systems, *Europhysics Letters*, vol. 5, pp. 973-977, 1987.

[18] N. Marwan, M.C. Romano, M. Thiel, and J. Kurths, Recurrence plots for the analysis of complex systems, *Phys. Rep.*, vol. 438, pp. 237-329, 2007.

[19] M.A. Little, P.E. McSharry, S.J. Roberts, D.A.E. Costello, and I.M. Moroz, Exploiting nonlinear recurrence and fractal scaling properties for voice disorder detection, *Biomed. Eng. Online*, vol. 6, 23, 2007.

[20] S. Boccaletti, V. Latora, Y. Moreno, M. Chavez, and D.U. Hwang, Complex networks: Structures and dynamics, *Phys. Rep.*, vol. 424, pp. 175-308, 2006.

[21] N. Marwan, J.F. Donges, Y. Zou, R.V. Donner, and J. Kurths, Complex network approach for recurrence analysis of time series, *Phys. Lett. A*, vol. 373, pp. 4246-4254, 2009.

[22] T.D. Pham, Fuzzy recurrence plots, *EPL (Europhysics Letters)*, vol. 116, 50008, 2016.

[23] L.A. Zadeh, Similarity relations and fuzzy orderings, *Information Sciences*, vol. 3, pp. 177-200, 1971.

[24] J.C. Bezdek, *Pattern Recognition with Fuzzy Objective Function Algorithms.* New York: Plenum Press, 1981.

[25] R.M. Haralick, K. Shanmugam, and I. Dinstein, Textural features of image classification, *IEEE Trans Systems, Man and Cybernetics*, vol. 3, pp. 610-621, 1973.

[26] L. Soh and C. Tsatsoulis, Texture analysis of SAR sea ice imagery using gray level co-occurrence matrices, *IEEE Trans Geoscience and Remote Sensing*, vol. 37, pp. 780-795, 1999.

[27] D.A. Clausi, An analysis of co-occurrence texture statistics as a function of grey level quantization, *Can. J. Remote Sensing*, vol. 28, pp. 45-62, 2002.

[28] D.J. Watts and S. Strogatz, Collective dynamics of 'small-world' networks, *Nature*, vol. 393, pp. 440-442, 1998.

[29] P. Martnez-Martn, A. Gil-Nagel, L.M. Gracia, J.B. Gomez, J. Martnez-Sarries, and F. Bermejo, Unified Parkinson's disease rating scale characteristics and structure. The Cooperative Multicentric Group, *Mov. Disord.*, vol. 9, pp. 76-83, 1994.

[30] J.A.K. Suykens, T.V. Gestel, J.D. Brabanter, B.D. Moor, and J. Vandewalle, *Least Squares Support Vector Machines*. Singapore: World Scientific, 2002.

[31] A.L.T. Tavares, G.S. Jefferis, M. Koop, B.C. Hill, T. Hastie, G. Heit, H.M. Bronte-Stewart, Quantitative measurements of alternating finger tapping in Parkinson's disease correlate with UPDRS motor disability and reveal the improvement in fine motor control from medication and deep brain stimulation, *Mov. Disord.*, vol. 20, pp. 1286-1298, 2005.

[32] T. Shimoyama, T. Ninchoji, K. Uemura, The finger-tapping test. A quantitative analysis, *Arch. Neurol.*, vol. 47, pp. 681-684, 1990.

[33] A. Fabretti, M. Ausloos, Recurrence plot and recurrence quantification analysis techniques for detecting a critical regime, *International Journal of Modern Physics C*, vol. 16, pp. 671-706, 2005.

[34] A. Fraser, H. Swinney, Independent coordinates for strange attractors from mutual information, *Phys Rev A*, vol. 33, pp. 1134-1140, 1986.

[35] M. Kennel, R. Brown, H. Abarbanel, Determing embedding dimension for phase space reconstruction using a geometrical construction, *Phys Rev A*, vol. 45, pp. 3403-3411, 1992.

[36] J.S. Iwanski, E. Bradley, Recurrence plots of experimental data: To embed or not to embed? *Chaos*, vol. 8, 861, 1998.

[37] S.E. Calvano, W. Xiao, D.R. Richards, R.M. Felciano, et al., A network-based analysis of systemic inflammation in humans, *Nature*, vol. 437, pp. 1032-1037, 2005.

[38] A.L. Hopkins, Network pharmacology: the next paradigm in drug discovery, *Nature Chemical Biology*, vol. 4, pp. 682-690, 2008.

[39] A.L. Barabasi, N. Gulbahce, J. Loscalzo, Network Medicine: A network-based approach to human disease, *Nature Reviews Genetics*, vol. 12, pp. 56-68, 2011.

[40] S.Y. Chan, J. Loscalzo, The emerging paradigm of network medicine in the study of human disease, *Circulation Research*, vol. 111, pp. 359-374, 2012.

[41] T. Ideker, R. Nussinov, Network approaches and applications in biology, *PLoS Comput Biol*, vol. 13, e1005771, 2017.

[42] T.R. Mhyre, J.T. Boyd, R.W. Hamill, K.A. Maguire-Zeiss, Parkinson's disease, *Sub-Cellular Biochemistry*, vol. 65, pp. 389-455, 2012.